PHYSICAL REVIEW D

PARTICLES AND FIELDS

THIRD SERIES, VOLUME 27, NUMBER 7 1 APRIL 1983

Search for production of narrow $\bar{p}p$ states with a 5-GeV/c $\bar{p}$ beam

J. Bensinger, L. Kirsch, W. Morris,* R. Poster, and P. Schmidt†
Brandeis University, Waltham, Massachusetts 02154

S. U. Chung, R. C. Fernow, H. Kirk, S. D. Protopopescu, and D. P. Weygand
Brookhaven National Laboratory, Upton, New York 11973

B. T. Meadows
University of Cincinnati, Cincinnati, Ohio 45221

J. R. Albright, R. Diamond, H. Fenker,‡ J. H. Goldman, V. Hagopian, and C. M. Jenkins
Florida State University, Tallahassee, Florida 32306

Z. Bar-Yam, J. Dowd, W. Kern, and M. Winik§
Southeastern Massachusetts University, North Dartmouth, Massachusetts 02747
(Received 19 October 1982)

A high-statistics search for the production of narrow $\bar{p}p$ states with a $\bar{p}$ beam at 5 GeV/c finds no evidence for such states from threshold up to 2.3 GeV. In particular, we set an upper limit (95% C.L.) of 9 nb for any state below 1.95 GeV with $\Gamma \leq 5$ MeV in the reaction $\bar{p}p \to \bar{p}p\pi^0$. Comparable limits are set for the reaction $\bar{p}p \to \bar{p}p(\rho+\omega)$ and inclusive $\bar{p}p$ production.

I. INTRODUCTION

The existence of narrow $\bar{N}N$ states, a subject of considerable interest to experimentalists and theorists alike, has been increasingly called into question over the last few years. The original observation of narrow states produced by baryon exchange[1] has been contradicted by subsequent experiments[2,3] while the existence of a narrow $\bar{p}p$ state ($\Gamma \lesssim 5$ MeV) with 1935-MeV mass seen in some formation[4,5] and production[6] experiments has not been confirmed by later ones.[7–9] However, the situation concerning the existence of this state is still unsettled. The data of Hamilton *et al.*[7] are consistent with the existence at that mass of an object broader ($\Gamma > 20$ MeV) than previously claimed with a cross section about 2% of the annihilation cross section. A new experiment[10] which claims much better resolution than Hamilton *et al.* seems to confirm the previous observation by Bruckner *et al.*[5] of a narrow state ($\Gamma \leq 4$ MeV) with cross section $\approx 5\%$ of the annihilation cross section. The most recent result is that of Sumiyoshi *et al.*[11] which seems inconsistent with the existence of either a narrow or broad object. Additional information is clearly still needed.

It is natural to expect that a state seen in $\bar{p}p$ formation should be observable in baryon-exchange processes and the most suitable reactions would be of the type

$$\bar{p}p \to (\bar{p}p)_f + X^0 , \tag{1}$$

where $(\bar{p}p)_f$ is fast in the laboratory system and X^0 is the recoil system. The use of a $\bar{p}$ beam allows one to study $\bar{p}p$ systems produced by baryon exchange in the forward direction (where detection and identification are easier) with relatively low beam momentum and low recoil mass so that the cross sections are large. We have reported on a preliminary analysis of reaction (1) with a $\bar{p}$ beam at 5 GeV/c in a previous publication.[3] In this paper we have dropped some restrictive requirements on the data, thereby increasing our acceptance, particularly at low $\bar{p}p$ masses, by as much as a factor of 20 without substantial increase in the background. We still ob-

serve no evidence for narrow states. Our present upper limits (95% C.L.) range from 10 nb below 1.95 GeV ($\Gamma \leq 5$ MeV) to 60 nb at 2.2 GeV ($\Gamma \leq 20$ MeV). The limits below 1.95 GeV correspond to $<8\%$ of the production cross section per 5 MeV and are 5 times lower than our previous publication.[3]

II. EXPERIMENTAL LAYOUT

The experiment was conducted at the Brookhaven National Laboratory multiparticle spectrometer (MPS) with a 5-GeV/c separated $\bar{p}$ beam incident on a 60-cm-long liquid-hydrogen target. The layout of the beam, known as the medium-energy separated beam (MESB), is described in detail in Ref. 12. Typical beam intensities achieved with the MESB tuned to 5-GeV/c antiprotons were 40 000 $\bar{p}$'s per pulse of the Alternating Gradient Synchrotron (AGS) with 2×10^{12} protons incident on the production target.

The purity of the $\bar{p}$ beam was typically 70%. Three gas Cherenkov counters $C1$, $C2$, and $C3$ filled with Freon 12 at 0.5, 0.5, and 61 psig, respectively, identified pions ($C1\cdot C2\cdot C3$), kaons ($\bar{C}1\cdot C2\cdot C3$), and antiprotons ($\bar{C}1\cdot\bar{C}2\cdot\bar{C}3$) in the beam. Contamination of valid events by misidentification of $\bar{p}$'s was negligible.

The beam line contained a beam spectrometer consisting of four proportional wire chambers (PWC's) surrounding the last 8° bending magnet in the beam-transport system. The beam-momentum resolution (σ) was 0.3%.

The apparatus for the experiment is shown in Fig. 1. It consists of the MPS magnet filled with an array of spark-chamber modules for measuring charged-particle trajectories, three multiwire proportional chambers for triggering purposes, and, downstream of the MPS magnet, a large high-pressure gas Cherenkov counter ($C7$) with γ threshold of 10 and two scintillator hodoscopes ($H5$ and $H7$). Detailed descriptions of the various elements of the MPS can be found in Ref. 13; here we include only a brief summary of the MPS configuration relevant to this experiment.

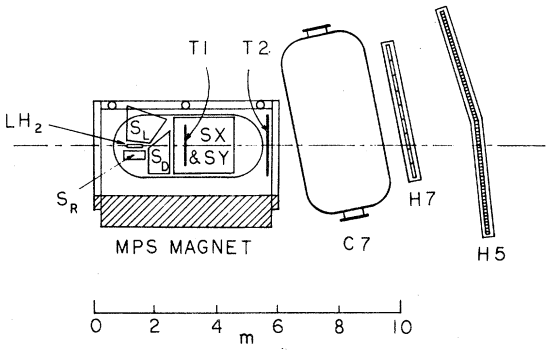

FIG. 1. Schematic diagram of the experimental layout. $T1$ and $T2$ are planar PWC's; $H7$ and $H5$ are scintillation-counter hodoscopes; $C7$ is the high-pressure Cherenkov counter. All these elements have been used in the triggers. S_L, S_R, and S_D are regions with capacitive-readout spark chambers. SX and SY are regions with magnetostrictive-readout spark chambers. The MPS magnet was set at 0.5 T (the direction of the field points into the paper).

Two types of spark chambers were used. Surrounding the target on the left, right, and directly downstream were three arrays of capacitive-readout chambers labeled S_L, S_R, and S_D in Fig. 1. S_L contained three chamber modules interspersed with three PWC's, S_R had two modules, and S_D had three modules. Each module had two X readouts (anode wires parallel to the magnetic field) and two Y readouts (anode wires perpendicular to the magnetic field); the PWC's in S_L read out in the X direction.

The bulk of the trajectory information came from the magnetostrictive-readout chamber modules filling the downstream half of the MPS magnet. There were eight SX modules containing $XUVX$ readouts each, and six SY modules with YY readouts. U,V denote chamber wires inclined $\pm15°$ with respect to the X wires.

The trigger PWC's $T1$ and $T2$ were located in the downstream half of the MPS magnet as shown in Fig. 1. The magnet was run at 5 kG central field during this experiment.

The high-pressure Cherenkov counter $C7$ was filled with 50 psig of Freon 12. It is a 3-m-diameter cylindrical vessel with optical components along the horizontal axis and symmetric with respect to its horizontal and midplane. Cherenkov light is reflected first from a plane mirror and then from an elliptical mirror before entering a bank of 160 photomultipliers, divided equally among top and bottom of the pressure vessel. Each photomultiplier is fitted

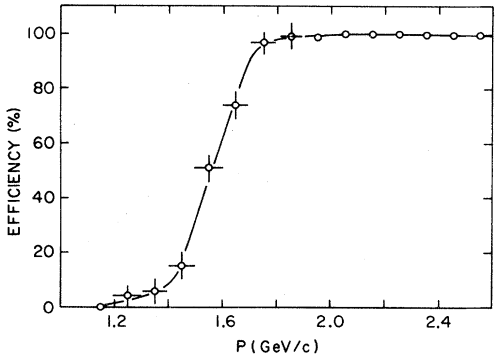

FIG. 2. Efficiency for detecting π's with $C7$ as a function of momentum (p).

with a lucite light pipe in the shape of a Winston cone,[14] which also acts as a pressure seal. This light pipe is connected inside the vessel to an aluminized Winston cone mirror guiding the Cherenkov light to the photocathode.

$H5$ is a 112-counter scintillation hodoscope with 2.5-in.-wide slats.

$H7$ is an 18-counter hodoscope, 9 top and 9 bottom, symmetric with respect to its horizontal midplane. Groups of 18 photomultipliers from $C7$ are ganged together in coincidence with a matching 18-in. slat from $H7$ to form $C7 \cdot H7$ and $\overline{C7} \cdot H7$ coincidences.

The trigger required a fast forward proton or K^+ with momentum greater than 1.2 GeV/c. The momentum of the trigger particle was selected by a three-dimensional coincidence-matrix logic system. It consisted of two random-access memories[15] (RAM1 and RAM2). The input signals to RAM1 were $(T1, T2, H5)$ and to RAM2 were $(T1, T2, \overline{C7} \cdot H7)$. The RAM1 system selected events having positive tracks in the required momentum and angular range. The RAM2 system ensured that the momentum-selected tracks went through the $C7$ fiducial volume and, by using $C7$ as a veto, rejected π^+'s accepted by RAM1. For momenta greater than 1.8 GeV/c the RAM1 and RAM2 coincidence rejected more than 99% of the π^+'s. In Fig. 2 we show the efficiency of $C7$ as a function of π^+ momentum. The π's were obtained from $K^- \to \pi^+\pi^-\pi^-$ decays using a 5-GeV/c K^- beam. Since the proton momentum distribution for our selected events peaks above 2.0 GeV, if we keep events with $p > 1.6$ GeV/c, the π^+ contamination in our whole sample will remain quite small.

III. DATA SELECTION

Table I lists the pertinent fluxes and rates of this $\bar{p}$-beam experiment and a comparison K^--beam experiment each at 5 GeV/c. While this paper focuses on the $\bar{p}$-beam data, some results from the K^- beam will also be presented, to demonstrate the quality of the data. The two experiments ($\bar{p}$ and K^-) were identical in all respects except for the beam. The triggers were processed through pattern recognition and track-fitting programs on the BNL CDC 7600 computer (where the processing time was about 250 msec per event).

The reaction studied was

$$\bar{p}p \to (\bar{p}p)_{\text{fast}} + X^0 ,$$

where X^0 is chiefly composed of neutral and charged pions. The event-selection process included the following requirements: (1) a reconstructed vertex inside the liquid-hydrogen target, (2) a positive nonpion particle with momentum > 1.6 GeV/c

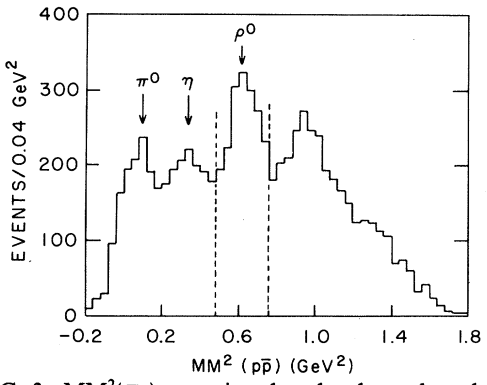

FIG. 3. $MM^2(\bar{p}p)$ assuming that the charged tracks are $\bar{p}$ and p and requiring that both tracks intersect $C7$ and have $p > 1.8$ GeV/c.

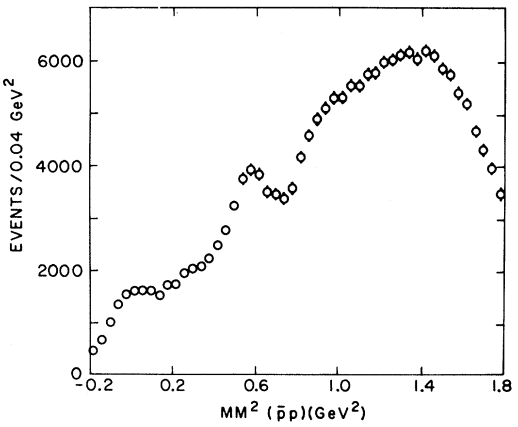

FIG. 4. $MM^2(\bar{p}p)$ for all combinations with $M(\bar{p}p) < 2.3$ GeV requiring only that the p satisfy the trigger requirements and have $p > 1.6$ GeV/c.

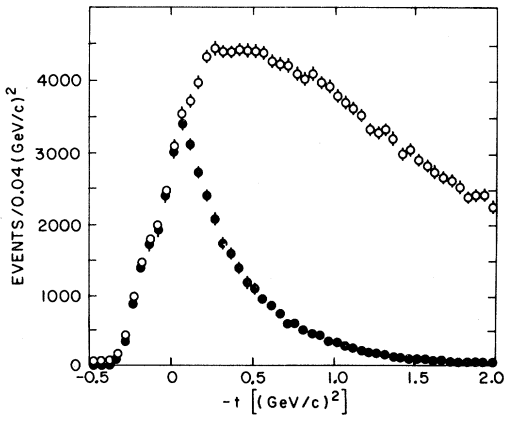

FIG. 5. Open circles (○) give the distribution of all the pairs in momentum transfer squared (t) requiring only that $M(\bar{p}p) < 2.3$ GeV. The closed circles (●) give the distribution for pairs for which $-0.25 < MM^2(\bar{p}p) < 0.76$ GeV^2.

satisfying the RAM trigger requirement, and (3) at least one additional negative reconstructed particle. A total of 192 000 events satisfied the above three criteria. The additional requirement that a negative track with momentum greater than 1.6 GeV/c go through $C7$, i.e., identifying the negative track as a nonpion, reduced the sample to 7000 events. This reduced sample of events was published in Ref. 3. In this paper that requirement will be dropped.

The purpose of this experiment is to look for narrow $\bar{p}p$ resonances. However, our identification and selection process will also accept $p\pi^-$ and pK^- as

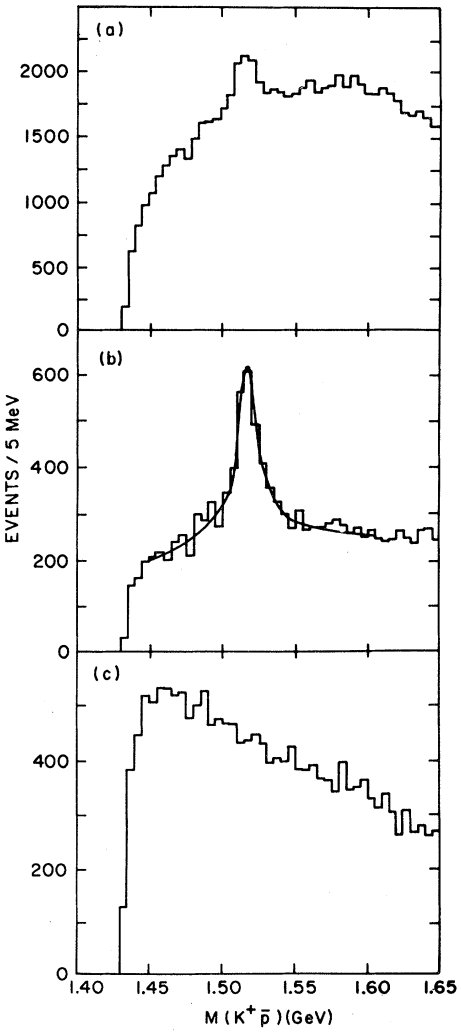

FIG. 6. (a) $M(\bar{p}K^+)$ for all pairs, satisfying $-t(\bar{p}\to\bar{p}K^+)<0.6$ (GeV/c)^2; (b) same as (a) but in addition, require $1.05<\mathrm{MM}^2(\bar{p}K^+)<1.45$ GeV^2 and include in case of ambiguity only the pair with lowest $-t(\bar{p}\to\bar{p}K^+)$; the solid curve is the result of a fit with a simple Breit-Wigner form plus quadratic background; (c) $M(\bar{p}K^+)$ for events requiring $-t(\bar{p}\to\bar{p}p)<0.6$ (GeV/c)^2 and $-0.15<\mathrm{MM}^2(\bar{p}p)<0.76$ GeV^2.

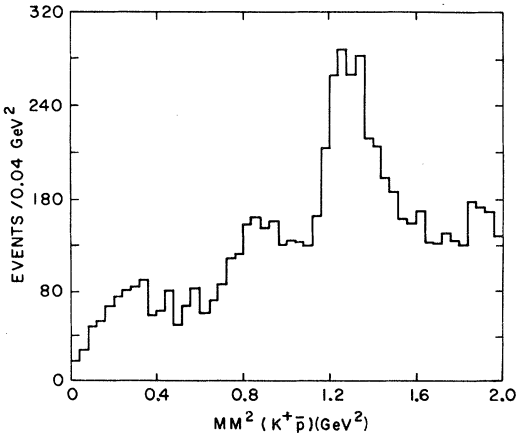

FIG. 7. $\mathrm{MM}^2(\bar{p}K^+)$ spectrum for events with $1.505<M(\bar{p}K^+)<1.530$ GeV and $-t(\bar{p}\to\bar{p}K^+)<0.6$ (GeV/c)^2.

well as $K^+\pi^-$, K^+K^-, and $\bar{p}K^+$. These unwanted combinations create a background, but a narrow $\bar{p}p$ peak should still be recognized. In order to reduce kinematic reflections from non-$\bar{p}p$ events, several cuts were applied to the data. The notation to be used for missing-mass calculations is as follows: For the reaction $\bar{p}p\to\bar{p}p+X^0$, $\mathrm{MM}^2(\bar{p}p)$ means the square of the mass of X^0 calculated as a missing mass with the masses of the positive and negative particles assumed to be p and $\bar{p}$, respectively. Figure 3 shows the missing-mass spectrum $\mathrm{MM}^2(p\bar{p})$ for the subsample where both the positive and negative particles are identified by $C7$ to be nonpions. The π^0, η and (ρ^0,ω) peaks are clearly evident. This

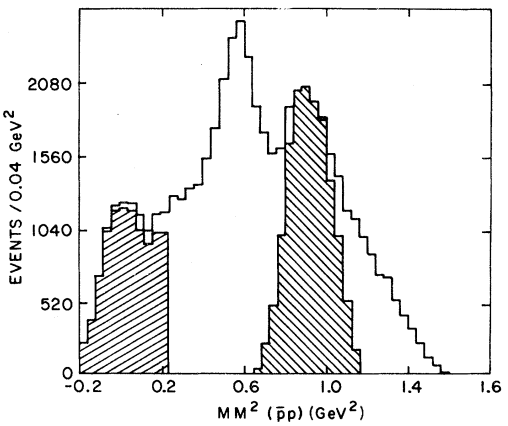

FIG. 8. $\mathrm{MM}^2(\bar{p}p)$ spectrum for events with $-t<0.6$ (GeV/c)^2 and $M(\bar{p}p)<2.3$ GeV. If more than one pair per event satisfies the requirements we only include the one with smallest $-t$. The shaded events under the first peak are two-prong events. The shaded events under the third peak are those for which $1.05<\mathrm{MM}^2(\bar{p}K^+)<1.45$ GeV^2.

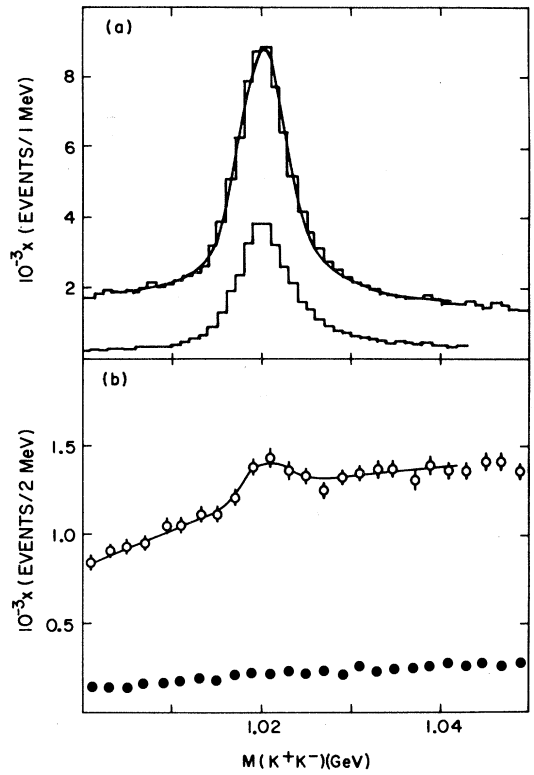

FIG. 9. (a) $M(K^+K^-)$ spectrum for $K^-p\to K^+K^-X$ and $K^-p\to K^+K^-\Lambda$. The solid line is a result of fit to a simple Breit-Wigner form keeping Γ fixed at 4.1 MeV plus a quadratic background; (b) $M(K^+K^-)$ spectrum (○) for $\bar{p}p\to K^+K^-+X$ all combinations. The solid curve is a fit to a simple Breit-Wigner form with parameters fixed to the values obtained in (a) plus a quadratic background. The closed circles (●) are the same events requiring $-0.15<\mathrm{MM}^2(\bar{p}p)<0.76$ GeV^2 and $-t(\bar{p}\to\bar{p}p)<0.6$ (GeV/c)^2.

sample of events is fairly clean, especially if $\mathrm{MM}^2(\bar{p}p)<0.76$ GeV^2 [because $\mathrm{MM}^2(\bar{p}K^+)$ and $\mathrm{MM}^2(pK^-)$ have thresholds at the $\Lambda/\bar{\Lambda}$) mass, respectively]. No narrow $\bar{p}p$ resonances were observed in this sample (see Ref. 3).

The acceptance for both the positive and the negative particle entering $C7$ is small (1 to 2%) and severely reduces the angular coverage. For this reason, in the following analysis only the positive particle is required to be identified by $C7$. However, 30% of the events contain more than one negative particle, and this leads to some combinatorial background. A series of cuts were applied to the data to enhance the $\bar{p}p$ signal relative to the background without drastically reducing the statistics of the signal. First, the mass of the $\bar{p}p$ system was restricted to be below 2.3 GeV; this reduces the combinatorial background. Figure 4 shows $\mathrm{MM}^2(\bar{p}p)$ for a total of 210 000 combinations from 180 000 events that satisfy this first cut. The π^0 and (ρ^0,ω) signals are clearly visible above large backgrounds. In order to reduce the K^-p and $\bar{p}K^+$ contamination, the second selection required that $-0.15<\mathrm{MM}^2(\bar{p}p)<0.76$ GeV^2. Events with $\bar{p}K^+$ or K^-p are accompanied by at least a Λ or $\bar{\Lambda}$, and will hence have a missing mass squared greater than 0.76 GeV^2. The lower bound of the second selection removes only K^+K^- or $K^+\pi^-$ events, without appreciably reducing the $\bar{p}p$ sample. Figure 5 shows the momentum transfer square (t_{pp}^-) from $\bar{p}$ to $\bar{p}p$ for events that pass the first cut (open circles) and the first and second cut (closed circles). Resonances in $\bar{p}p$ should be produced by baryon exchange and should be peripheral. The second cut clearly favors the low-t events, thereby enhancing peripheral $\bar{p}p$ production. A third cut, $-t_{pp}^-<0.6$ (GeV/c)^2, was then applied, reducing the sample to 58 000 events of which only 5% have more than one $\bar{p}p$ possibility due to multiple negative tracks. For the remaining discussion, if more than one $\bar{p}p$ hypothesis exists, then the one with the lowest $|t_{pp}^-|$ will be used.

One way to measure how well the $\bar{p}K^+$ and K^-p possibilities have been removed is to study the hypotheses $\bar{p}p\to\bar{p}K^+X^0$. Figure 6 shows various $\bar{p}K^+$ mass spectra. In Fig. 6(a), only the third cut, $-t(\bar{p}\to\bar{p}K^+)<0.6$ (GeV/c)^2, has been applied. The $\bar{\Lambda}(1520)\to\bar{p}K^+$ is unquestionably visible. The additional requirement $1.05<\mathrm{MM}^2(\bar{p}K^+)<1.45$ GeV (i.e., selecting missing Λ) greatly enhances the $\bar{\Lambda}(1520)$ as shown in Fig. 6(b). Figure 7 shows the $\mathrm{MM}^2(\bar{p}K^+)$ spectrum for events in the $\bar{\Lambda}(1520)$ peak, i.e., $1.505<M(\bar{p}K^+)<1.530$ GeV and $-t(\bar{p}\to\bar{p}K^+)<0.6$ (GeV/c)^2. The Λ peak is greatly enhanced and the number of Λ's are close to the number of $\bar{\Lambda}(1520)$ events indicating that most of the $\bar{\Lambda}(1520)$ come from the reaction $\bar{p}p\to\bar{\Lambda}(1520)\Lambda$. If instead the second and third cuts are applied, i.e., $-0.15<\mathrm{MM}^2(\bar{p}p)<0.76$ GeV^2 together with $-t_{pp}^-<0.6$ (GeV/c)^2, no $\bar{\Lambda}(1520)$ peak is observed [see Fig. 6(c)]. This shows that the three cuts effectively remove all $\bar{p}K^+$ events. We thus conclude that after cuts the contamination of $\bar{p}K^+$ events in the $\bar{p}p$ sample is negligible. A similar argument also applies to the pK^- events. Figure 8 shows the $\mathrm{MM}^2(\bar{p}p)$ for events that pass the first and third cuts. The π^0 and (ρ,ω) peaks are clearly evident. The third peak at 0.9 to 1.0 GeV^2 is the reflection of the Λ from the $\bar{p}K^+$ events. The cross-hatched events under this third peak correspond to the same events where $1.05<\mathrm{MM}^2(\bar{p}K^+)<1.45$ GeV^2, i.e., events in the Λ missing-mass peak. Clearly the third peak is almost entirely due to $\bar{p}K^+$ events and so a $\mathrm{MM}^2(\bar{p}p)<0.76$ GeV^2 cut eliminates most of this background. The low number of events with $\mathrm{MM}^2(\bar{p}p)<-0.15$ GeV^2 indicates that the back-

ground from K^+K^- and $K^+\pi^-$ events is small (since for those events the $\bar{p}p$ hypothesis can lead to negative MM^2). The cross-hatched events under the first peak, $-0.2 < MM^2(\bar{p}p) < 0.25$ GeV^2, are two-prong events. Over 97% of the events in that region are two prong, as expected if they come mostly from the reaction $\bar{p}p \to \bar{p}p\pi^0$.

The $\bar{\Lambda}(1520)$ peak can be used to check the experimental rms resolution. A fit to the $\bar{p}K^+$ spectrum with a Breit-Wigner form plus a quadratic background (assuming $\sigma = 3$ MeV, the calculated value of the resolution) gives $m = 1517 \pm 1$ MeV and $\Gamma = 13 \pm 2$ MeV, compared to the world average values of $1519.5 + 1.5$ MeV and 15.5 ± 1.5 MeV, respectively.[16] A better check of our resolution at low masses comes from reconstructed $\phi \to K^+K^-$ decays. Figure 9(a) shows events for $K^-p \to (K^+K^- + X^0)$ and $(K^+K^- + \Lambda)$ in 1-MeV bins in the ϕ region. Fitting these events to a Breit-Wigner form plus quadratic background and assuming $\Gamma = 4.1$ MeV, gave $\sigma = 2.6$ MeV and $m = 1020.1 \pm 0.2$ MeV, to be compared to the world average value of 1019.6 ± 0.2 MeV. This shows that any systematic errors in the mass calculation are small. The σ obtained from the fit agrees well with the σ calculated from track errors which gave a value of 2.5 MeV. Figure 9(b) shows the K^+K^- spectrum for the hypothesis $\bar{p}p \to K^+K^- + X^0$ with no cuts. Most of the events are not K^+K^-, but a small ϕ signal can be seen at the right mass and with the expected width, above a very large background. At the peak the signal-to-background ratio is 1/7.

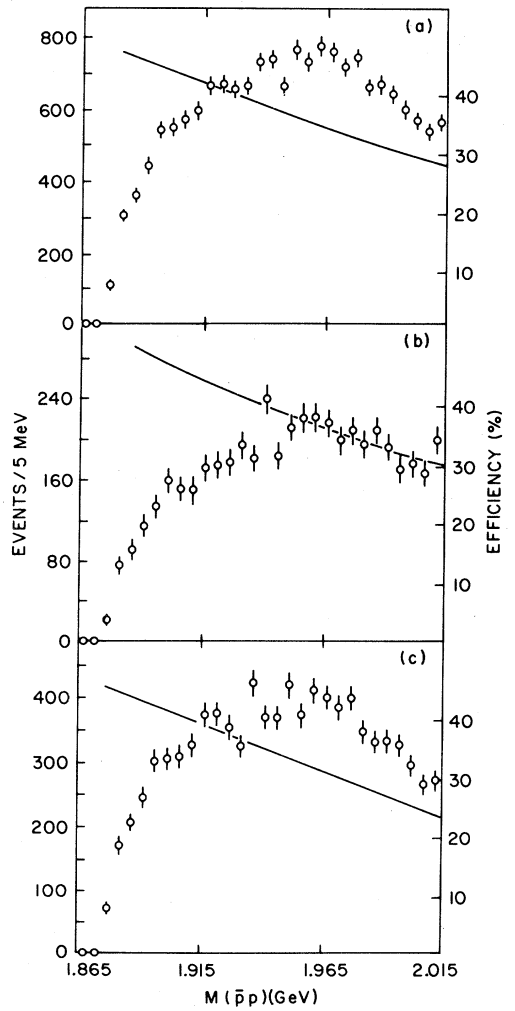

FIG. 10. (a) $M(\bar{p}p)$ spectrum for $-0.15 < MM^2(\bar{p}p) < 0.76$ GeV^2; (b) $M(\bar{p}p)$ for $\bar{p}p \to \bar{p}p\pi^0$, π^0 defined as two prongs with $-0.15 < MM^2(\bar{p}p) < 0.2$ GeV^2; (c) $M(\bar{p}p)$ for $\bar{p}p \to \bar{p}p(\rho+\omega)$, $\rho+\omega$ defined as $0.44 < MM^2(\bar{p}p) < 0.76$ GeV^2. All spectra require $-t < 0.6$ (GeV/c)^2. The solid curves indicate the calculated efficiency.

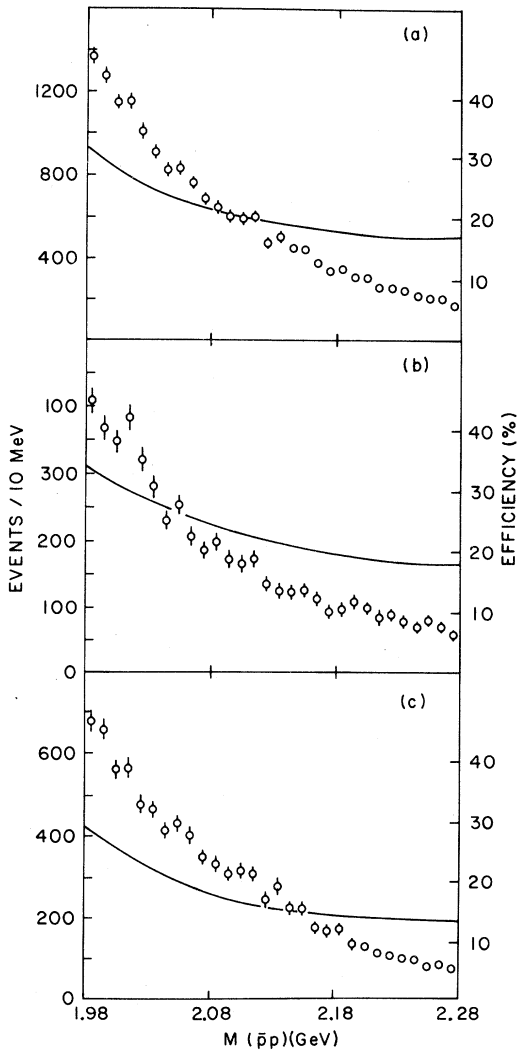

FIG. 11. (a) Same as Fig. 10(a); (b) same as Fig. 10(b); (c) same as Fig. 10(c).

Figure 9(b) also shows the same spectrum after requiring cuts two and three, i.e., $-0.15 < \mathrm{MM}^2(\bar{p}p) < 0.76$ GeV and $-t_{pp}^{-} < 0.6$ $(\mathrm{GeV}/c)^2$; there is no evidence of any ϕ production, consistent with the expectation that after these three cuts the contribution from events other than $\bar{p}p$ is negligible.

IV. LIMITS ON NARROW $\bar{p}p$ STATES

In Figs. 10 and 11 we show the $\bar{p}p$ mass spectra, in 5-MeV bins below 2.0 GeV and 10-MeV bins above 2.0 GeV, after requiring $-0.15 < \mathrm{MM}^2(\bar{p}p) < 0.76$ GeV^2, $-t_{pp}^{-} < 0.6$ $(\mathrm{GeV}/c)^2$, and, if more than one combination satisfies those cuts, keeping only the one with lowest $-t_{pp}^{-}$. Clearly no significant structure is present for these events, nor is there any if we select $\bar{p}p\pi^0$, defined as two-prong events with $-0.15 < \mathrm{MM}^2(\bar{p}p) < 0.2$ GeV^2, or $\bar{p}p(\rho+\omega)$, defined as events with $0.44 < \mathrm{MM}^2(\bar{p}p) < 0.76$ GeV^2.

To calculate the acceptances, Monte Carlo events were generated for reactions $\bar{p}p \to \bar{p}pX^0$ as functions of $\bar{p}p$ mass and $\bar{p}p$ missing mass with a $e^{3.0t}$ production distribution and isotropic angular decay distribution. The generated events were put through the trigger requirements and the reconstruction programs. The geometrical acceptance and program efficiency is quite large, ranging from 65% near threshold to 20% above 2.1 GeV [these include the $-t < 0.6$ GeV^2/c^2 cut]. An additional 30% loss occurs from inefficiencies in the trigger elements, beam losses, etc. The final efficiencies as a function of mass are shown in Figs. 10 and 11; these efficiencies assume isotropic decay-angular distributions. In Figs. 12 and 13 we show the $\cos\theta$ decay distribution in the Jackson frame ($\cos\theta_J$) and the t_{pp}^{-} distributions for 5 mass regions; θ_J is defined as the angle between the beam and the outgoing $\bar{p}$ in the $\bar{p}p$ rest frame. Also included are the calculated efficiencies as a function of $\cos\theta_J$ and t. One can see from Fig. 12 that, although the data are not isotropic, given the good angular acceptance when $M(\bar{p}p) < 2.0$ GeV estimated upper limits for narrow $\bar{p}p$ states will be fairly insensitive to the decay angular distribution. This is not the case for $M(\bar{p}p) > 2.0$ GeV, where upper limits can change significantly if very asymmetrical distributions are expected (possible if there are large interference effects). In the latter case the upper limits given in Table I need to be recalculated using the efficiency as a function of $\cos\theta_J$ given in Fig. 12.

To check the efficiency calculation we used the reaction $K^-p \to \phi\Lambda$, $\phi \to K^+K^-$, for which we have a fairly clean signal and the contribution from $K^-p \to \phi\Sigma^0$ seems to be small (see Fig. 14). The overall flux for the K^- data is 11 nb^{-1} and the efficiency for reconstructing $K^-p \to \phi\Lambda$ is $20 \pm 1\%$. This is substantially lower than for low-mass $\bar{p}p$ pairs because of K decays. A fit to the observed events gives $28\,500 \pm 200$ ϕ's from which we obtain a cross section (corrected for branching ratio) of 27 ± 2

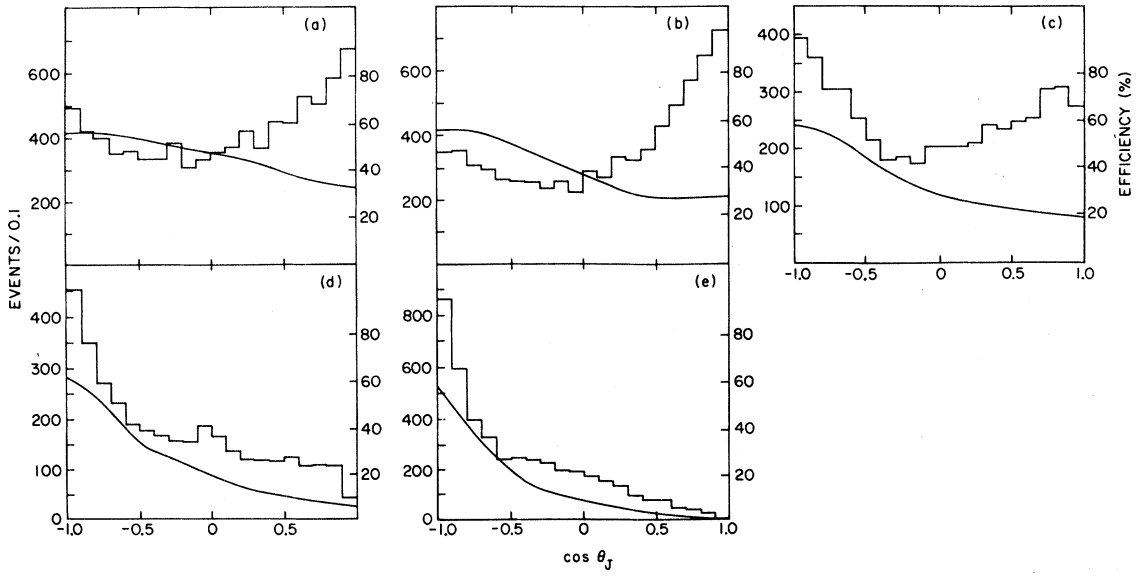

FIG. 12. $\cos\theta$ distribution in the Jackson frame (θ angle between $\bar{p}$ beam and outgoing $\bar{p}$ in $\bar{p}p$ rest frame) for $-0.15 < \mathrm{MM}^2(\bar{p}p) < 0.76$ GeV^2 $-t < 0.6$ $(\mathrm{GeV}/c)^2$ and (a) $M(\bar{p}p) < 1.95$ GeV, (b) $1.95 < M(\bar{p}p) < 2.0$ GeV, (c) $2.0 < M(\bar{p}p) < 2.05$ GeV, (d) $2.05 < M(\bar{p}p) < 2.1$ GeV, (e) $2.1\ \mathrm{GeV} < M(\bar{p}p) < 2.2$ GeV. The solid curves indicate the calculated efficiencies.

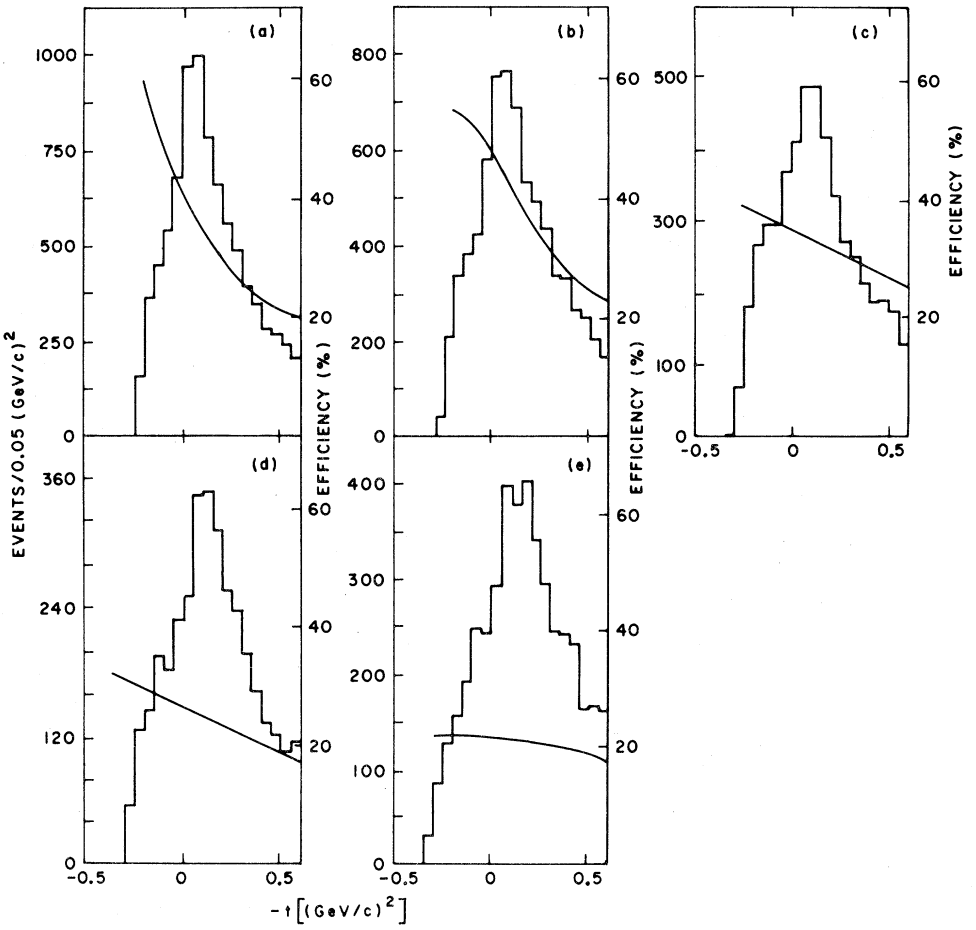

FIG. 13. t distributions for $-0.15 < MM^2(\bar{p}p) < 0.76$ GeV^2 and (a) $M(\bar{p}p) < 1.95$ GeV, (b) $1.95 < M(\bar{p}p) < 2.0$ GeV, (c) $2.0 < M(\bar{p}p) < 2.05$ GeV, (d) $2.05 < M(\bar{p}p) < 2.1$ GeV, (e) $2.1 < M(\bar{p}p) < 2.2$ GeV.

μb, the error comes from uncertainties in the Monte Carlo calculations. The estimated cross section for this reaction from the world compilation[17] is 36 ± 5 μb, compatible with ours.

The total flux for the $\bar{p}$ beam is 6.0 nb^{-1} and using the acceptances shown in Figs. 10 and 11 we obtain 2σ upper limits given in Table II. Between the threshold and 1.95 GeV our effective mass resolu-

TABLE I. Data rates for the $\bar{p}$ beam and the companion K^--beam experiment.

	$\bar{p}$	K^-
Particles per pulse	40 000	15 000
Number of hours	70	300
Total flux	2.7×10^9	4.5×10^9
Trigger rate	$\frac{1}{3500}$	$\frac{1}{1500}$
Number of triggers	7.7×10^5	3×10^6

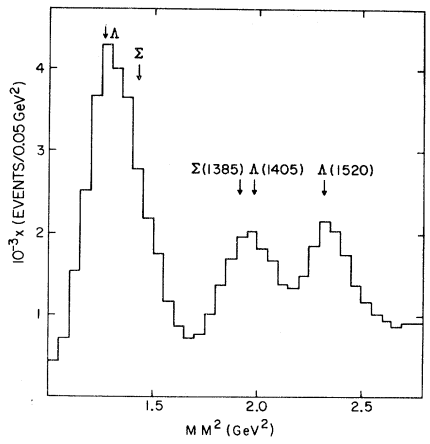

FIG. 14. $MM^2(K^+K^-)$ spectrum from reaction $K^-p \to K^+K^- + X$ requiring $1.014 < M(K^+K^-) < 1.026$ GeV.

TABLE II. Production-cross-section upper limits (95% confidence level).

$M(\bar{p}p)$ (GeV)	$\Gamma <$ (MeV)	$\sigma(nb)$ π^0	$\rho+\omega$	"Inclusive"
<1.95	5	9	15	20
1.95–2.0	10	17	26	36
2.0–2.05	10	19	31	39
2.05–2.2	20	26	55	58

tion varies from 2.0 to 3.0 MeV so we can give limits for states with $\Gamma \leq 5$ MeV. They range from 9 nb for $\bar{p}p\pi^0$ to 20 nb for $\bar{p}p$ inclusive (inclusive are events with $0.15 < \mathrm{MM}^2 < 0.76$ GeV^2). The resolution varies from 3 to 6 MeV between 1.95 and 2.05 GeV; thus we give limits in that region for $\Gamma \leq 10$ MeV, while by 2.2 GeV it is 10 MeV so limits are given for $\Gamma \leq 20$ MeV above 2.05 GeV. It is noteworthy to point out that the limit in the S region (1935 MeV) is $<8\%$ of the "inclusive" cross section. This is to be compared with the observation of the S as 5% of the annihilation cross section in formation experiments.[5,10] As pointed out earlier (see Fig. 12) the very good angular acceptance below 1.95 GeV implies that our limit is independent of the angular distribution. Above 2.05 GeV it is important to keep in mind that these limits are for isotropic decay angular distributions. The variation can be substantial if the decay angular distribution is highly asymmetric.

V. CONCLUSION

A high-statistics search for the production of narrow $\bar{p}p$ states with a $\bar{p}$ beam at 5 GeV/c was conducted with negative results. The experiment had good resolution and particularly good and uniform acceptance at low masses, ≤ 1.95 GeV. These enabled us to set upper limits (95% C.L.) of 9 nb for $\bar{p}p \to \bar{p}p\pi^0$, 15 nb for $\bar{p}p \to \bar{p}p(\rho+\omega)$, and 20 nb for $\bar{p}p \to \bar{p}pX^0$ [where X^0 is defined by $-0.15 < \mathrm{MM}^2(\bar{p}p) < 0.76$ GeV^2] for the production of states with $\Gamma \leq 5$ MeV. From 1.95 to 2.05 GeV our limits ranged from 20 to 40 nb for $\Gamma \leq 10$ MeV and above 2.05 GeV from 30 to 60 nb for $\Gamma \leq 20$ MeV. The upper limits are typically a factor of 5 lower than previously published for the same reactions.[3]

ACKNOWLEDGMENTS

We acknowledge with pleasure the support of the MPS personnel, the personnel of the Experimental Planning and Support Division and of the On-Line Data Facility, and the AGS operating staff. This research was supported in part by the U. S. Department of Energy and by the National Science Foundation.

*Present address: Corning Medical, Medfield, Massachusetts.
†Present address: Automatix, Burlington, Massachusetts 01803.
‡Present address: Fermi National Laboratory, Batavia, Illinois.
§Present address: Brookhaven National Laboratory, Upton, New York 11973.

[1]P. Benkheiri *et al.*, Phys. Lett. 68B, 483 (1977).
[2]R. M. Bionta *et al.*, Phys. Rev. Lett. 44, 909 (1980); A. S. Carroll *et al.*, *ibid.* 44, 1572 (1980); S. Kooijman *et al.*, 45, 316 (1980); S. U. Chung *et al.*, *ibid.* 45, 1611 (1980).
[3]S. U. Chung *et al.*, *ibid.* 46, 395 (1981).
[4]A. S. Carroll *et al.*, Phys. Rev. Lett. 32, 247 (1974); T. E. Kalogeropoulos and G. S. Tzanakos, *ibid.* 34, 1047 (1975); V. Chaloupka *et al.*, Phys. Lett. 61B, 487 (1976).
[5]W. Bruckner *et al.*, Phys. Rev. Lett. 67B, 222 (1977).
[6]D. Aston *et al.*, Phys. Lett. 93B, 517 (1980); C. Daum *et al.*, *ibid.* 90B, 475 (1980).
[7]R. Hamilton *et al.*, Phys. Rev. Lett. 44, 1179 (1980); 45, 1182 (1980).
[8]T. Kamae *et al.*, Phys. Rev. Lett. 44, 1439 (1980); E. Jastrzembski *et al.*, Phys. Rev. D 23, 2784 (1981); D. I. Lowenstein *et al.*, *ibid.* 23, 2788 (1981).
[9]C. Daum *et al.*, Phys. Lett. 100B, 439 (1981).
[10]C. Amsler et al., Report No. CERN-EP/82-93 (unpublished).
[11]T. Sumiyoshi *et al.*, Phys. Rev. Lett. 49, 628 (1982).
[12]C. T. Murphy and J. T. Fox, Brookhaven National Laboratory Report No. EPSS-73-2, MPS Note No. 22, 1973 (unpublished).
[13]E. D. Platner *et al.*, in *Proceedings of the International Conference on Instrumentation for High Energy Physics, Frascati, Italy, 1973,* edited by S. Stipcich (Laboratori Natzionali del Comitato Natzionale per l'Energia Nucleare, Frascati, Italy, 1973), p. 673; S. J. Lindenbaum, in *Proceedings of the Fourth International Symposium on $\bar{N}N$ Interactions, Syracuse University, 1975,* edited by T. E. Kalogeropoulos and K. C. Wali (Syracuse University, Syracuse, New York, 1975), Vol. II, p. VII–19.
[14]H. Hinterberger and R. Winston, Rev. Sci. Instrum. 37, 1094 (1966).
[15]E. D. Platner *et al.*, IEEE Trans. Nucl. Sci. 24, 1225 (1977).
[16]Particle Data Group, Rev. Mod. Phys. 52, S1 (1980).
[17]High Energy Reactions Analysis Group, Report No. CERN-HERA 79-02, 1979 (unpublished).